Chinese Physics Letters

LETTER

Switchable Auxetic Piezoelectricity in Rhombohedral Relaxor Ferroelectrics

Cite as: He-Meng Sun *et al*. 2026 *Chin. Phys. Lett.* **43** 120702

Recommended Articles

Switchable Band Topology and Geometric Current in Sliding Bilayer Elemental Ferroelectric
Zhuang Qian, Zhihao Gong, Jian Li, Hua Wang, and Shi Liu
Chin. Phys. Lett. **42**, 070715 (2025)

Rhombohedrally-Distorted Orthorhombic $Hf_{0.5}Zr_{0.5}O_{2-x}$ Stabilized by Cooperative Oxygen Vacancies and Lattice Distortions
Lei Liao *et al*.
Chin. Phys. Lett. **43**, 030702 (2026)

Hole-Doped Nonvolatile and Electrically Controllable Magnetism in van der Waals Ferroelectric Heterostructures
Xinxin Jiang, Zhikuan Wang, Chong Li, Xuelian Sun, Lei Yang, Dongmei Li, Bin Cui, and Desheng Liu
Chin. Phys. Lett. **41**, (2024)

Double Helix of Atomic Displacements in Ferroelectric $PbTiO_3$
Yihao Hu, and Shi Liu
Chin. Phys. Lett. **42**, 120707 (2025)

Tunable Insulator–Metal Transitions and Flat Bands in Domain-Wall-Engineered Monolayer In_2Se_3
Laiyuan Su, Zhigang Gui, and Li Huang
Chin. Phys. Lett. , (2026)

A series journal of Chinese Physical Society distributed by IOP Publishing

Chinese Physics Letters

Chin. Phys. Lett. **43** 120702 (2026)

LETTER

DOI: 10.1088/0256-307X/43/12/120702
CSTR: 32039.14.0256-307X.43.12.120702

Switchable Auxetic Piezoelectricity in Rhombohedral Relaxor Ferroelectrics

He-Meng Sun(孙和猛)[1,2], Hang-Bo Zhang(张杭波)[2], Zhi Tan(谭智)[3,*], and Ming-Min Yang(杨明敏)[1,2,*]

[1]School of Emerging Technology, University of Science and Technology of China, Hefei 230026, China
[2]Hefei National Laboratory, Hefei 230088, China
[3]College of Materials Science and Engineering, Sichuan University, Chengdu 610065, China

[*]Corresponding authors. Email: tanzhi0838@scu.edu.cn; mingminyang@hfnl.cn

Piezoelectric materials typically exhibit opposite longitudinal and transverse mechanical responses under an electric field, reflecting the electromechanical analogue of a positive Poisson's ratio. Auxetic piezoelectricity, in which longitudinal and transverse coefficients share the same sign, has recently emerged as an unconventional electromechanical response; yet its intrinsic realization and electrical tunability in relaxor ferroelectrics with complex domain structures remain elusive. Here, we demonstrate intrinsic and electrically switchable auxetic piezoelectricity in rhombohedral relaxor ferroelectric $Pb(Mg_{1/3}Nb_{2/3})O_3$-$PbTiO_3$ by combining first-principles calculations and quantitative piezoelectric measurements. Density functional perturbation theory reveals that a positive transverse piezoelectric response is symmetry-allowed in the rhombohedral phase and primarily originates from internal-strain contributions associated with cooperative Pb-O displacements. Experiments on single-domain $(111)_{pc}$-oriented crystals confirm the existence of an intrinsic auxetic state. Beyond the single-domain limit, *in situ* bias-dependent measurements reveal continuous and reversible electric-field-driven switching between auxetic and conventional piezoelectric states within the same crystal. A tensor-rotation-based multi-domain model quantitatively reproduces the bias-dependent response and identifies domain redistribution, enabled by the large shear piezoelectric coefficient, as the microscopic origin of the switching behavior. These findings establish auxetic piezoelectricity as an intrinsic and electrically programmable response in rhombohedral relaxor ferroelectrics, providing a general route toward reconfigurable electromechanical functionalities.

Piezoelectric materials deform mechanically in response to an external electric field, typically exhibiting opposite signs between the longitudinal and transverse piezoelectric coefficients [1,2]. Consequently, an electric field applied along the polarization direction induces expansion (or contraction) along the longitudinal axis while simultaneously causing contraction (or expansion) in the transverse directions, resembling the electromechanical analogue of a positive Poisson's ratio. Although this response underpins a wide range of applications, including actuators, sensors, and energy-harvesting devices [3], the intrinsic sign opposition between longitudinal and transverse strains leads to partial cancellation of electromechanical deformation, thereby limiting the achievable electromechanical coupling efficiency and overall device performance [4].

To overcome the intrinsic sign opposition between longitudinal and transverse piezoelectric responses, the concept of the auxetic piezoelectric effect has recently been proposed to describe a counterintuitive piezoelectric response in which the longitudinal and transverse piezoelectric coefficients share the same sign, leading to simultaneous expansion or contraction in all directions under an electric field [5]. First-principles studies have shown that such an auxetic piezoelectric response is symmetry-allowed in a limited number of materials, including orthorhombic ferroelectric HfO_2 [5] and rhombohedral nitride perovskites $LaWN_3$ [6,7]. Experimentally, auxetic piezoelectricity has been demonstrated in semiconductor heterostructures [8,9], where orientation-dependent electrostriction induces an interfacial auxetic response, and more recently in bulk Aurivillius ferroelectric ceramics [10]. However, these studies remain largely confined to idealized single-domain predictions, interfacial systems, or well-poled ferroelectric ceramics, leaving it unclear whether auxetic piezoelectricity can be intrinsically realized and reversibly controlled in bulk relaxor ferroelectrics with complex domain structures, which are more directly relevant to scalable electromechanical applications.

Rhombohedral ferroelectric perovskites offer a natural platform for auxetic piezoelectricity, as their *3m* tensor permits a positive transverse response along the polar axis [6,11]. However, realizing this response in realistic relaxor ferroelectrics is nontrivial because the measured piezoelectric coefficients depend not only on the intrinsic tensor but also on domain configuration and its field-driven evolution. Relaxor-based $Pb(Mg_{1/3}Nb_{2/3})O_3$-$PbTiO_3$ (PMN-PT), a technologically important rhombohedral perovskite widely used in high-performance electromechanical devices [1], provides an ideal model system to address this issue. In rhombohedral PMN-PT, polarization vectors distributed along equivalent $\langle 111\rangle_{pc}$ directions form multiple domain variants [12], whose electric-field-driven redistribution can substantially alter the tensorial projection of piezoelectric coefficients onto a certain laboratory frame [13]. This effect is further amplified by the large intrinsic piezoelectric anisotropy [14], exceptionally strong shear coefficient d_{15} [2] and low domain-wall energy [15] of relaxor ferroelectrics, suggesting that domain redistribution may not only modify the magnitude of the apparent piezoelectric response but also reconfigure the sign relationship between longitudinal and transverse coefficients. These features identify rhombohedral PMN-PT as an ideal model system for examining how an intrinsic auxetic tensor response emerges in a real relaxor ferroelectric and how it can be electrically reconfigured through domain redistribution.

Here, we first use first-principles calculations on PMN-25PT as the representative rhombohedral piezoelectric system, and then we conduct quantitative piezoelectric measurements on commercially accessible rhombohedral PMN-30PT single crystals to investigate detailed properties of auxetic piezoelectricity. We first show that a positive transverse piezoelectric response is intrinsic to the rhombohedral *3m* piezoelectric tensor and originates from internal-strain contributions associated with cooperative Pb-O displacements. Using $(111)_{pc}$-oriented single crystals, we experimentally verify an intrinsic auxetic

Received 29 July 2026; accepted 19 October 2026; published 17 November 2026
© 2026 Chinese Physical Society and IOP Publishing Ltd. All rights, including for text and data mining, AI training, and similar technologies, are reserved.

Check for updates

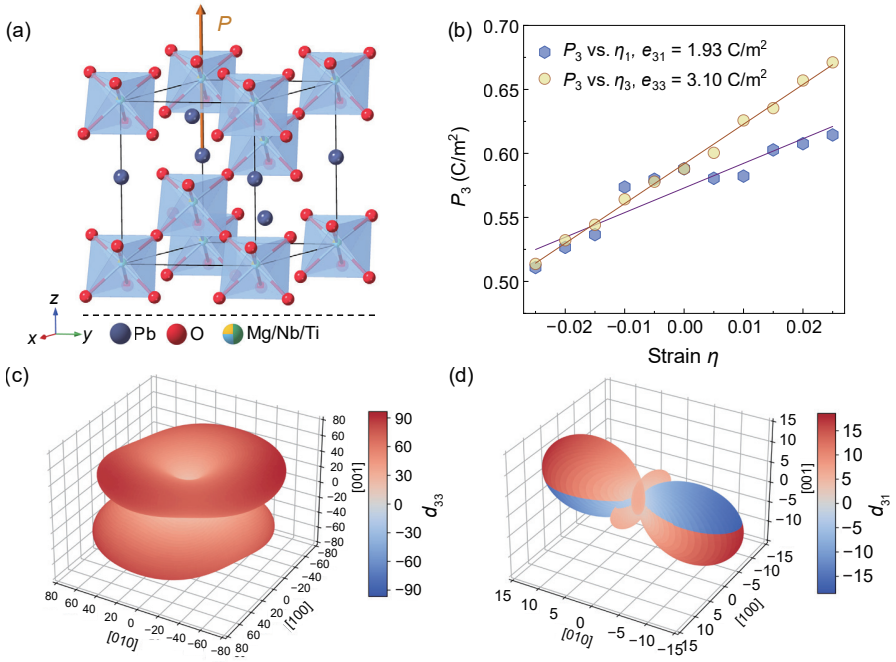

Fig. 1. Crystal structure and first-principles-calculated piezoelectric coefficients of rhombohedral PMN-PT. (a) Crystal structure of R3m PMN-25PT in the hexagonal setting. (b) Polarization P_3 as a function of uniaxial strains η_1 and η_3. (c) and (d) Spherical polar plots showing the crystallographic-orientation dependence of the (c) d_{33} and (d) d_{31} at $\varphi = 0°$.

piezoelectric state in the single-domain limit. We then demonstrate that electric-field-driven domain reconfiguration enables continuous and reversible switching between auxetic and conventional piezoelectric responses within the same crystal. Finally, a tensor-rotation-based multi-domain model quantitatively describes the bias-dependent evolution of the apparent piezoelectric coefficients and clarifies the role of domain redistribution in governing the switching behavior. Beyond demonstrating switchable auxetic piezoelectricity, this work highlights domain reconfiguration as a powerful lever for engineering unconventional electromechanical responses in technologically relevant ferroelectrics.

Results

First-Principles Analysis of Auxetic Piezoelectricity in Rhombohedral PMN-PT

To establish whether auxetic piezoelectricity is intrinsically allowed in rhombohedral relaxor ferroelectrics, we first analyze the piezoelectric response of single-domain PMN-25PT using first-principles calculations. Figure 1(a) illustrates the crystal structure of rhombohedral PMN-25PT in the hexagonal setting, with the spontaneous polarization oriented along the $[001]_h$ direction. We then evaluate the evolution of the out-of-plane polarization component P_3 under uniaxial strains applied parallel and perpendicular to the polarization direction. As shown in Fig. 1(b), P_3 increases linearly with both in-plane and out-of-plane strains, yielding positive piezoelectric stress coefficients e_{31} = 1.93 C/m^2, and e_{33} = 3.10 C/m^2. The corresponding piezoelectric strain coefficients, obtained from the calculated piezoelectric stress tensor and elastic constants [Table S1 of the Supplementary Materials (SM)] using density functional perturbation theory (DFPT) [16–18], are d_{31}= 4.36 pC/N and d_{33}= 15.14 pC/N, both of which are positive. Owing to the *3m* point-group symmetry of rhombohedral PMN-PT, the two in-plane transverse coefficients are equivalent ($d_{31} = d_{32}$). Therefore, only d_{31} is discussed here. Further details of the computational model, including the model construction and atomic configurations, are provided in Fig. S1 of the SM.

To further assess the orientation dependence of the transverse and longitudinal piezoelectric responses, we examine the effective piezoelectric coefficients in an arbitrary measurement frame via tensor transformation. Figures 1(c) and 1(d) present the three-dimensional polar spherical distributions of the effective d_{33} and d_{31}, respectively. Notably, the effective d_{33} remains positive over the entire orientation space, while d_{31} is not only positive along the polar axis but also remains positive within a finite angular range around it. The robustness of this positive transverse response is further supported by supplementary orientation-dependent analyses (Figs. S2 and S3 of the SM), which show that d_{31} remains positive in the low-θ region for all in-plane rotations, where θ denotes the polar angle between the measurement direction and the polarization axis. Details of the coordinate transformation and tensor rotation procedure are provided in Fig. S4 of the SM. These results establish that auxetic piezoelectricity is intrinsically encoded in the rhombohedral piezoelectric tensor of PMN-25PT, motivating a microscopic analysis of its underlying physical origin.

To elucidate the microscopic origin of the anomalous positive transverse piezoelectric response, we decompose the transverse piezoelectric coefficient into clamped-ion and internal-strain contributions according to [19, 20]

$$e_{31} = e_{31}^{(0)} + \sum_s \frac{e}{\Omega} Z_{33,s}^{*} \frac{\partial u_{3,s}}{\partial \eta_1}, \tag{1}$$

where $e_{31}^{(0)}$ is the clamped-ion term and the second term, denoted as $e_{31}^{(i)}$, represents the internal-strain contribution arising from the relaxation of internal atomic coordinates under an applied macroscopic transverse strain η_1. The clamped-ion contribution is found to be small and negligible ($e_{31}^{(0)} \approx 0.01$ C/m^2), indicating that the observed positive transverse response is dominated by internal-strain effects. Figure 2(a) summarizes the element-resolved out-of-plane displacement change rate $\partial u_3/\partial \eta_1$ extracted from first-principles calculations (Fig. S5 of the SM). Pb exhibits the largest positive displacement under in-plane tensile strain, whereas O displays an opposite-signed displacement, resulting in a pronounced relative Pb-O motion. To assess how these strain-induced displacements contribute to polarization, we examine the Born effective charges Z_{33}^{*} of individual ions [Fig. 2(b)]. The Born effective charges are significantly larger than the nominal ionic charges, reflecting the mixed ionic–covalent bonding character of PMN-25PT and indicating that even moderate atomic displacements can induce substantial polarization changes along the polar axis.

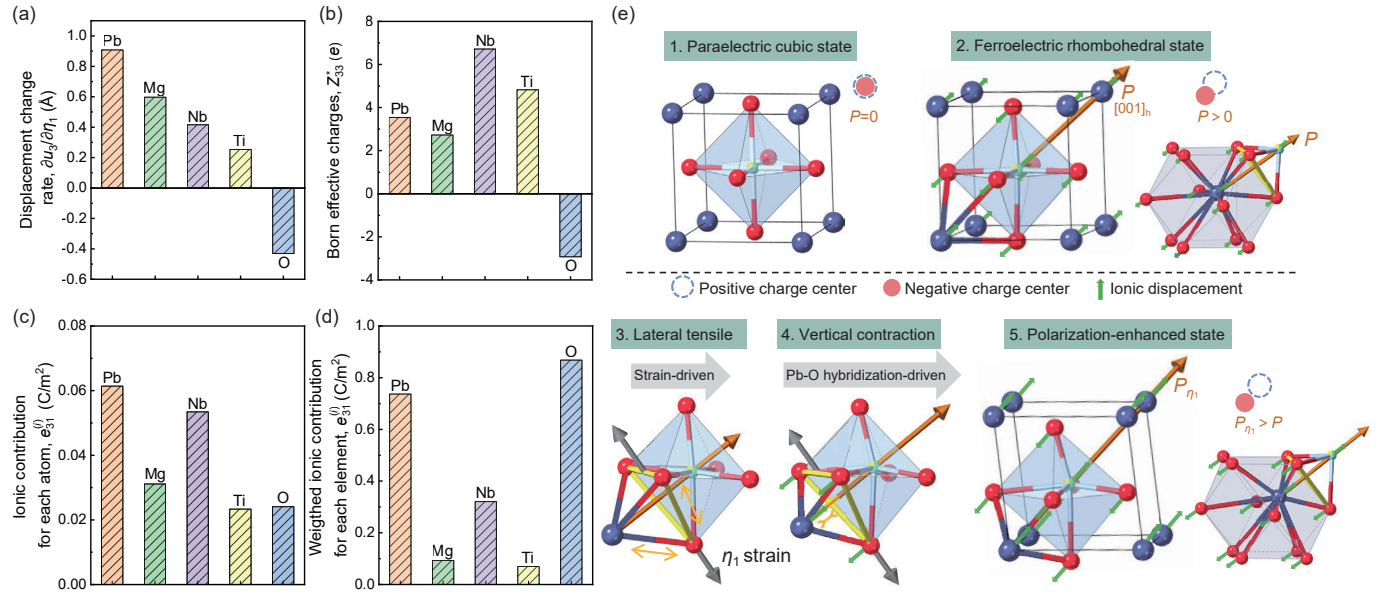

Fig. 2. Microscopic origin of the anomalous transverse piezoelectric response in rhombohedral PMN-25PT. (a) Element-resolved out-of-plane atomic displacement response $\partial u_3/\partial\eta_1$ under in-plane tensile strain η_1. (b) Born effective charges Z^*_{33} of individual ions. (c) Ionic contributions for each atom to the internal-strain piezoelectric coefficient $e^{(i)}_{31}$. (d) Stoichiometry-weighted ionic contributions for each element to $e^{(i)}_{31}$. (e) Schematic illustration of the strain-driven polarization evolution along the polar $[001]_h$ direction: (1) paraelectric cubic state with zero polarization; (2) ferroelectric rhombohedral state with spontaneous polarization; (3) lateral-tensile-induced expansion of the basal oxygen triangle and elongation of in-plane Pb-O bonds; (4) Pb-O-hybridization-driven vertical contraction; and (5) polarization-enhanced state with further separation of positive and negative charge centers.

The combination of $\partial u_3/\partial\eta_1$ and Z^*_{33} yields the atom-resolved ionic contributions to the internal-strain piezoelectric coefficient $e^{(i)}_{31}$ [Fig. 2(c)]. After accounting for the stoichiometry of different atomic species, the weighted ionic contributions $e^{(i)}_{31}$ for each element [Fig. 2(d)] reveal that the transverse piezoelectric response is governed primarily by Pb-O relative motion, underscoring the central role of the stereochemically active Pb-O bonding environment.

This microscopic mechanism is schematically illustrated in Fig. 2(e). In the paraelectric cubic state, the positive and negative charge centers coincide, resulting in zero macroscopic polarization. Upon entering the ferroelectric rhombohedral state, cooperative ionic displacements separate the charge centers along the polar $[001]_h$ direction and generate spontaneous polarization. Structurally, the perovskite lattice consists of corner-sharing BO_6 octahedra (B = Mg/Nb/Ti), while Pb occupies the A site within a PbO_{12} cage, forming a flexible Pb-O polyhedral environment. Upon application of an in-plane tensile strain η_1, the basal oxygen triangle of the Pb-centered polyhedron expands laterally, elongating the in-plane Pb-O bonds and strengthening Pb-O hybridization. The enhanced Pb-O hybridization then drives a vertical contraction of the Pb-O framework, promoting further separation of the positive and negative charge centers along $[001]_h$ and thereby enhancing the out-of-plane polarization. Overall, these results reveal that the positive transverse piezoelectric response originates predominantly from the internal-strain contribution, whereby transverse strain induces cooperative Pb-O displacements that enhance the polarization along the polar axis. In addition, Nb-O hybridization and the corresponding distortion of the basal oxygen triangle in the Nb-centered octahedra can produce a similar effect along $[001]_h$, although this contribution is secondary in PMN-25PT because B site cooperative displacements are often disrupted by the chemical disorder among Nb, Mg, and Ti cations. It is worth noting that the total B-site contribution is approximately 0.484 C/m^2, corresponding to 65.7% of the Pb contribution. This substantial contribution indicates that B-site displacements also play an important role in determining the positive e_{31} and therefore cannot be neglected in the perovskite ferroelectrics.

Hence, this auxetic piezoelectric response may not be unique to PMN-25PT. In lead-free rhombohedral perovskite ferroelectrics $BaTiO_3$, similar B-site-dominated mechanisms are also expected to give rise to auxetic piezoelectricity (Fig. S6 of the SM). As shown in Fig. S7 of the SM, first-principles calculations for several representative rhombohedral perovskites consistently yield positive transverse (e_{31}) and longitudinal (e_{33}) piezoelectric coefficients. Previous calculations also report auxetic piezoelectric effects in rhombohedral $BaTiO_3$, though the signs of d_{31} and d_{33} are both negative due to the different adopted ferroelectric polarization/sign convention [11, 18]. These results suggest that auxetic piezoelectricity may be broadly present in rhombohedral polar perovskites, driven by tensile-strain-enhanced polar-axis polarization. Motivated by these predictions, we next turn to experimental verification in a single-domain rhombohedral PMN-PT crystal.

Experimental Verification of Auxetic Piezoelectricity in Single-Domain PMN-PT

In order to experimentally verify the auxetic piezoelectric response in a $(111)_{pc}$-oriented rhombohedral single crystal, we conducted piezoelectric measurements in a commercially available PMN-30PT single crystal (Fig. S8 of the SM), where the rhombohedral phase is also robust at room temperature. The $PbTiO_3$ content (x) of the PMN-PT crystal composition was determined from dielectric temperature spectra (Fig. S9 of the SM). Figures 3(a) and 3(b) show reciprocal space mappings (RSMs) around the $(112)_{pc}$ reflection before and after electrical poling. In the unpoled state [Fig. 3(a)], the diffraction pattern exhibits an elongated and split intensity distribution, characteristic of the coexistence of multiple equivalent rhombohedral domain variants. Electrical poling was carried out by applying a DC bias of 800 V/mm at 200 ℃, followed by cooling to room temperature while maintaining the electric field. After poling, the RSM collapses into a single, well-defined diffraction spot [Fig. 3(b)], indicating the formation of a single-domain state with a uniform polarization orientation. The establishment of a single-domain configuration is further corroborated by vector piezoresponse force microscopy (PFM) measurements (Fig. S10 of the SM). Both vertical and lateral PFM amplitude and phase images evolve from spatially heterogeneous contrast in the unpoled state to uniform contrast after poling, confirming homogeneous polarization in both out-of-plane and in-plane components.

Having established a single-domain state, we directly probe the longitudinal and transverse piezoelectric responses of the poled PMN-30PT single crystal using a quasi-static direct piezoelectric measurement. A sinusoidal compressive stress is homogeneously applied along

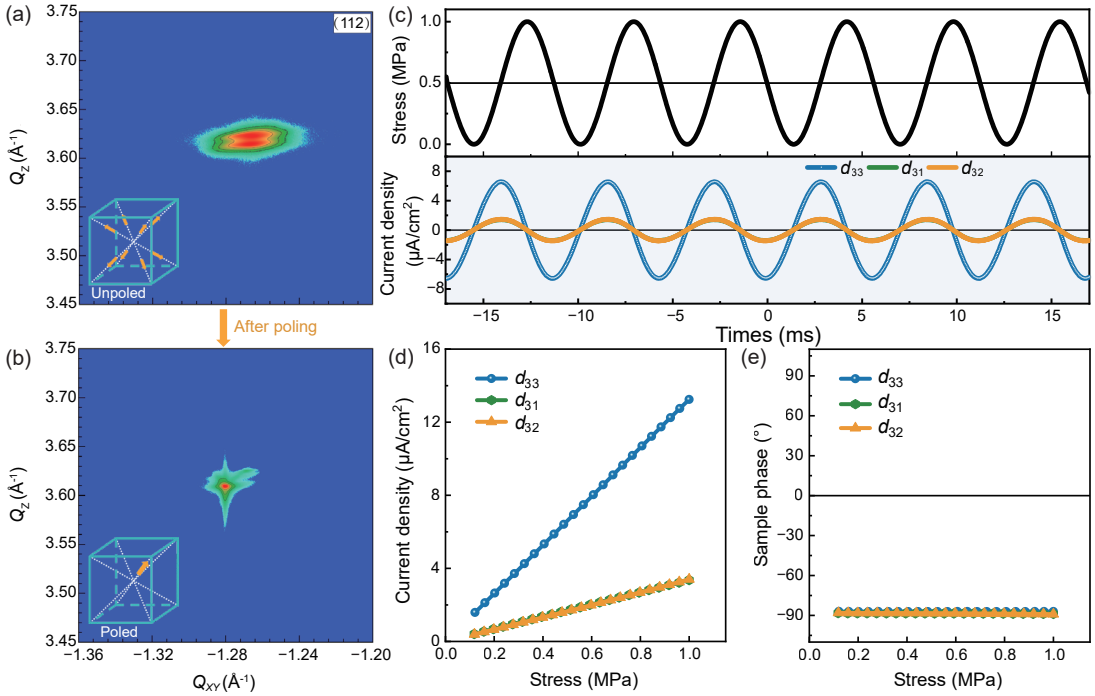

Fig. 3. Domain structure and experimental piezoelectric characteristics in $(111)_{pc}$-oriented PMN-30PT single crystal. (a) and (b) RSMs around the $(112)_{pc}$ reflection in (a) unpoled and (b) poled states, confirming the formation of a single-domain configuration after electrical poling. Insets illustrate the corresponding domain configurations. (c) Waveform of applied sinusoidal compressive stress (top panel), and the corresponding induced short-circuit current density (bottom panel), with stress respectively applied parallel (d_{33}, along $[111]_{pc}$) and perpendicular (d_{31}, along $[11\bar{2}]_{pc}$, and d_{32}, along $[1\bar{1}0]_{pc}$) to the direction of polarization. (d) Stress-dependent amplitude and (e) stress-dependent phase of the short-circuit current density induced by piezoelectric d_{33}, d_{31}, and d_{32} at a measurement frequency of 177.7 Hz.

selected crystallographic directions, with the induced short-circuit current recorded *in situ*. Stress applied parallel to the polarization direction along $[111]_{pc}$ measures the longitudinal d_{33} response, whereas stresses applied perpendicular to the polarization along $[11\bar{2}]_{pc}$ and $[1\bar{1}0]_{pc}$ probe the transverse d_{31} and d_{32} responses, respectively. The experimental sign convention, including the polarization direction, electrode connection, stress directions, and current direction, is defined in Fig. S11 of the SM. Under this convention, $\Delta\phi = \phi_{stress} - \phi_{current} = -90^\circ$ and $+90^\circ$ correspond to positive and negative d_{3j}, respectively. Figure 3(c) shows the applied stress waveform together with the corresponding induced current densities. All three current responses exhibit $\Delta\phi \approx -90^\circ$, confirming positive d_{33}, d_{31}, and d_{32}, and thus the auxetic piezoelectric response.

To quantify the piezoelectric coefficients, the current density amplitude is measured as a function of applied stress [Fig. 3(d)]. In all loading configurations, the current density exhibits a linear dependence on stress, consistent with the linear piezoelectric relation $J_3 = 2\pi f d_{3i}\sigma_i$. From the slopes, we extract $d_{33} = 118$ pC/N, $d_{31} = 24.5$ pC/N, and $d_{32} = 24.6$ pC/N. The corresponding phase responses remain constant over the entire stress range [Fig. 3(e)], indicating stable and intrinsic piezoelectric behavior without phase reversal. Frequency-dependent measurements performed under fixed stress conditions (Fig. S12 of the SM) further confirm the reproducibility and robustness of the response. Together, these results establish a robust intrinsic auxetic piezoelectric response in single-domain PMN-30PT.

The experimentally extracted coefficients, $d_{31} = 24.5$ pC/N, and $d_{33} = 118$ pC/N, are approximately 5.6 and 7.8 times larger, respectively, than the corresponding 0 K DFPT values. This difference reflects the distinct physical regimes represented by the two approaches, that is, the DFPT captures the intrinsic lattice response of an ordered structural model at 0 K [18, 21], whereas room-temperature relaxor PMN-PT additionally involves chemical-disorder-induced local structural heterogeneity [22] and thermally activated polarization fluctuations associated with dynamic polar nanoregions [23, 24], which can enhance the effective polarization susceptibility and piezoelectric response. The individual contributions of these effects cannot be separately quantified from the present measurements. Nevertheless, the positive d_{31} obtained both from the 0 K calculation and the room-temperature single-domain experiment indicates that the intrinsic positive transverse response is preserved across these two regimes.

Notably, the auxetic piezoelectric response in PMN-30PT, in which the transverse coefficients share the same sign as the longitudinal one, results in a strongly enhanced hydrostatic piezoelectric coefficient $d_h = d_{33} + d_{31} + d_{32}$. Benefiting from the simultaneously large magnitudes of all three components, PMN-PT exhibits a large hydrostatic coefficient of $d_h \approx 167$ pC/N, which is expected to substantially exceed those reported in previously demonstrated auxetic piezoelectric systems [8, 9].

For comparison, direct piezoelectric measurements are also carried out on poled multi-domain $(001)_{pc}$-oriented rhombohedral PMN-27PT single crystals (Fig. S13 of the SM). The $(001)_{pc}$-oriented crystal exhibits a conventional piezoelectric response, clearly distinct from the auxetic behavior of the $(111)_{pc}$-oriented crystal. These results establish the single-domain $(111)_{pc}$-oriented single crystal as a unique single crystal platform for auxetic piezoelectricity, and the exceptional domain-engineering flexibility of relaxor ferroelectrics enables us to examine how this crystal responds to an external electric field.

Domain-Engineered Switching of Auxetic and Conventional Piezoelectric States

We perform *in situ* quasi-static piezoelectric measurements under a DC bias on an initially unpoled $(111)_{pc}$-oriented PMN-30PT single crystal, to probe how the piezoelectric response evolves under an applied electric field. The experimental configuration is schematically illustrated in Fig. 4(a), where a slowly varying DC electric bias is applied across the crystal, while a small sinusoidal compressive stress is superimposed to probe the instantaneous piezoelectric current response.

Figure 4(b) and Fig. S14 of the SM show the electric-field dependence of the apparent piezoelectric coefficients d_{33}, d_{31}, and d_{32}. These coefficients are extracted from the measured piezoelectric current density under a small AC stress using a fixed measurement configuration and thus represent apparent values defined within the

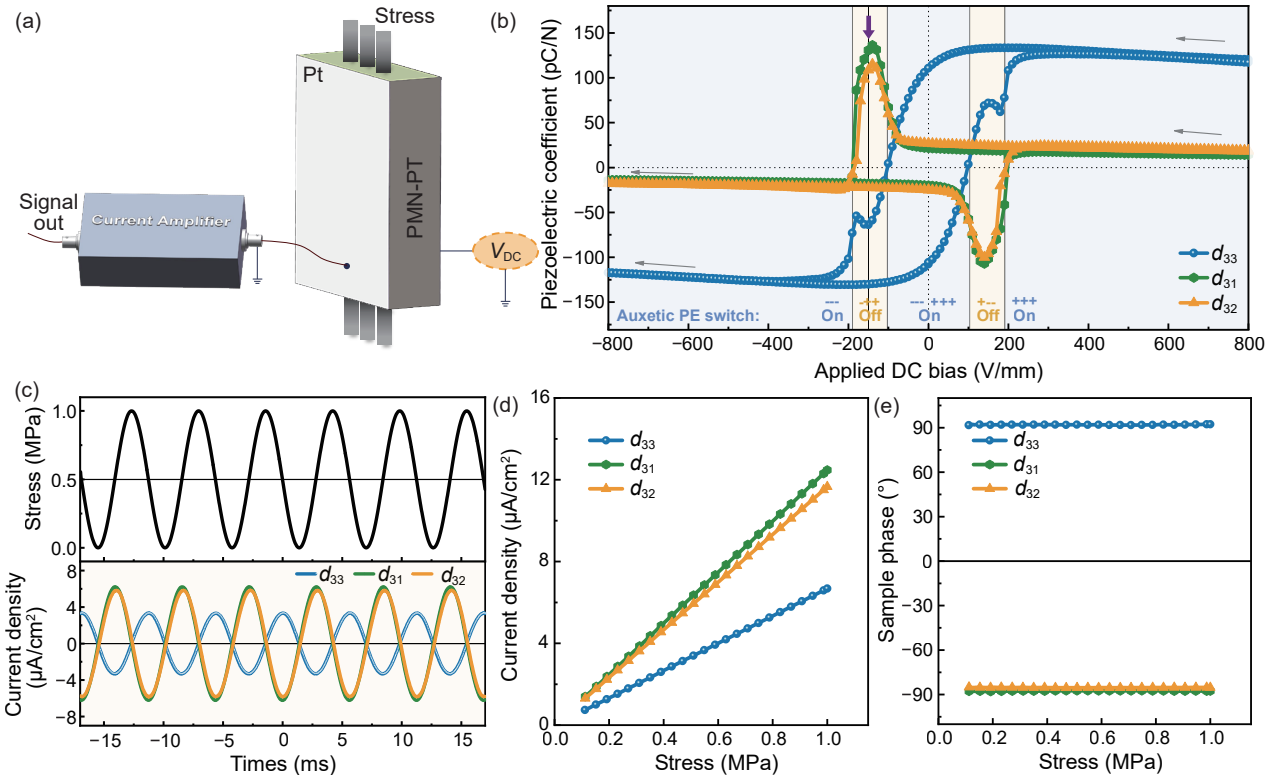

Fig. 4. Electric-field-driven switching between auxetic and conventional piezoelectric states in $(111)_{pc}$-oriented PMN-30PT single crystal. (a) Schematic of the measurement geometry for *in situ* quasi-static piezoelectric characterization under an applied DC electric bias. (b) Electric-field-dependent apparent piezoelectric coefficients d_{33}, d_{31}, and d_{32}, extracted from the measured piezoelectric current density, showing reversible switching between auxetic and conventional piezoelectric states. (c) Waveform of the applied sinusoidal compressive stress (top panel) and the corresponding induced short-circuit current density (bottom panel), measured at the conventional piezoelectric state marked by the purple arrow in panel (b). (d) and (e) Stress-dependent amplitudes and phases of the current density for d_{33}, d_{31}, and d_{32}, indicating stable and well-defined piezoelectric responses in the selected conventional state.

present experimental framework. Here, we define an effective ratio $v_{13} = -d_{31}/d_{33}$, which serves as an analogue of the mechanical Poisson's ratio in piezoelectric systems [25]. At large positive or negative fields, the crystal evolves into a single-domain state, where the polarization aligns along opposite out-of-plane directions, resulting in a corresponding reversal in the signs of d_{33}, d_{31}, and d_{32}. In these two high-field states, the transverse coefficients d_{31} and d_{32} share the same sign as the longitudinal coefficient d_{33}, corresponding to an auxetic piezoelectric state with a negative value of v_{13}. Within an intermediate bias window, the crystal enters a distinct regime in which d_{31} and d_{32} reverse sign relative to d_{33}, indicating a transition to a conventional piezoelectric state with a positive value of v_{13}. Strikingly, this transition is accompanied by a strong enhancement of the transverse response, with $1\bar{1}0$ increasing from ~24 pC/N in the auxetic regime to values as large as ~136 pC/N. At the boundaries between these two regimes, where either the transverse coefficients vanish (d_{31}, $d_{32} = 0$) or the longitudinal coefficient is suppressed ($d_{33} = 0$), the crystal passes through true bulk states corresponding to $v_{13} = 0$ and effectively infinite v_{13}, analogous to zero and effectively infinite Poisson's ratio [4, 26, 27], revealing the continuous electric-field tunability of the electromechanical coupling (Fig. S15 of the SM).

To verify the stability and intrinsic nature of the conventional piezoelectric regime identified in Fig. 4(b), we examine the piezoelectric response at a representative bias point (−150 V/mm). After electrically driving the crystal to this bias point, the DC bias is removed, leaving the sample in a relatively stable multi-domain configuration. Figure 4(c) shows the applied sinusoidal compressive stress together with the corresponding short-circuit current densities, confirming that the conventional piezoelectric response persists after removal of the DC bias. The current density amplitudes scale linearly with the applied stress for all three piezoelectric coefficients [Fig. 4(d)]. From the slopes, the coefficients are determined to be $d_{33} = -59.5$ pC/N, $d_{31} = 110.8$ pC/N, and $d_{32} = 104.3$ pC/N. The corresponding phase responses remain constant over the entire stress range [Fig. 4(e)], confirming a robust and well-defined piezoelectric response in the multi-domain state. Frequency-dependent measurements (Fig. S16 of the SM) further confirm the reproducibility of the conventional piezoelectric response. These results demonstrate that v_{13} in rhombohedral PMN-PT, serving as an electromechanical counterpart to Poisson's ratio, is not only switchable but continuously programmable by an external electric field, offering a powerful route toward programmable electromechanical functionality. To uncover the microscopic origin of this switching behavior, we analyze the bias-driven evolution of domain configurations and the corresponding changes in the apparent piezoelectric response.

To elucidate the microscopic origin of the electric-field-driven switching between auxetic and conventional piezoelectric responses in $(111)_{pc}$-oriented rhombohedral PMN-30PT single crystals, we formulate a tensor-rotation-based multi-domain averaging model to describe the experimentally observed switching behavior. Rhombohedral PMN-30PT possesses eight symmetry-related polarization variants, which can be grouped into four domain families: 0°, 71°, 109°, and 180° [13, 28]. Owing to the crystallographic misorientation of these variants with respect to the fixed laboratory frame, their intrinsic piezoelectric tensors are rotated into the laboratory coordinates, and the macroscopic piezoelectric response is obtained by averaging the rotated tensors weighted by the corresponding domain volume fractions. Within this model, the apparent longitudinal and transverse piezoelectric coefficients for a $(111)_{pc}$-oriented crystal can be expressed in compact form as

$$d'_{33} = (n_1 - n_4)d_{33} + (n_2 - n_3)\frac{1}{27}(d_{33} + 8d_{31} + 8d_{15}), \quad (2)$$

$$d'_{31} = (n_1 - n_4)d_{31} + (n_2 - n_3)\frac{1}{27}(4d_{33} + 5d_{31} - 4d_{15}), \quad (3)$$

where n_1–n_4 denote the volume fractions of the 0°, 71°, 109°, and 180° domain groups, respectively, with $n_1 + n_2 + n_3 + n_4 = 1$. Here,

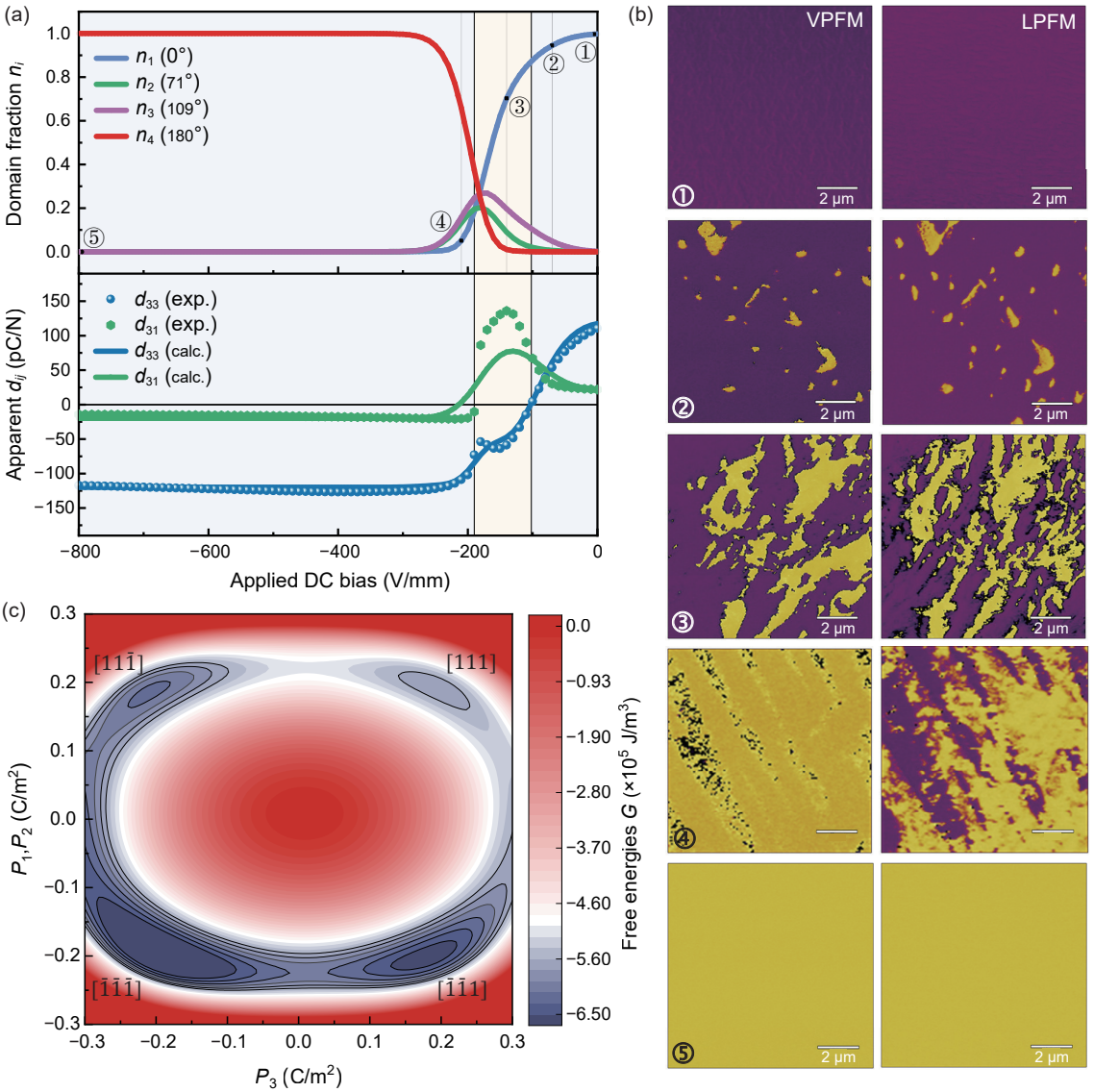

Fig. 5. Microscopic origin of electric-field-driven auxetic–conventional piezoelectric switching in rhombohedral PMN-30PT. (a) Bias-dependent domain volume fractions and apparent piezoelectric coefficients calculated using a tensor-rotation and domain-averaging model, capturing the microscopic redistribution of polarization variants under DC bias. (b) Vector PFM phase images (VPFM and LPFM) acquired at representative bias points marked in (a), directly visualizing the microscopic domain evolution that underpins the observed piezoelectric switching. (c) Contour map of the free energy projected onto the $(1\bar{1}0)_{pc}$ plane for PMN-30PT at a bias electric field of –0.2 MV/m, showing multiple local minima associated with thermodynamically competitive rhombohedral polarization states.

d_{33}, d_{31}, and d_{15} are the intrinsic piezoelectric coefficients of a single-domain $(111)_{pc}$-oriented rhombohedral PMN-30PT crystal. The full tensor-rotation derivation and domain volume-fraction averaging are provided in SM.

To quantitatively connect the domain-averaging model with the room-temperature measurements, we use $d_{33} = 120$ pC/N and $d_{31} = 20$ pC/N together with the experimentally reported shear piezoelectric coefficient $d_{15} \approx 4100$ pC/N [29] for rhombohedral PMN-PT. Substituting these values into Eqs. (2) and (3), the experimentally measured bias-dependent apparent piezoelectric coefficients are quantitatively reproduced, as shown in Fig. 5(a). Since the piezoelectric coefficients alone do not uniquely specify all four domain fractions, representative bias-dependent vector PFM states [see Fig. 5(b)] are used to constrain the initial domain populations. The fractions n_1–n_4 are then iteratively optimized under $0 \le n_i \le 1$, $\sum_i n_i = 1$, and continuous evolution with bias, yielding the domain-population trajectory shown in Fig. 5(a).

A prominent feature of the model is the dominant role of the exceptionally large shear piezoelectric coefficient d_{15} characteristic of rhombohedral PMN-PT [29, 30]. Through tensor rotation, this shear component is projected into both d'_{33} and d'_{31}, rendering the apparent piezoelectric response highly sensitive to the populations of non-collinear domains and enabling the switching between auxetic and conventional piezoelectric behavior. In the intermediate bias region, the rapid reduction of the initial 0° domain fraction accompanied by an increase in the 109° domain population leads to a pronounced enhancement of d'_{31}, while simultaneously driving d'_{33} to zero and even reversing its sign. The auxetic piezoelectric response characteristic of the single-domain state is thus converted into a conventional piezoelectric response stabilized by a multi-domain intermediate configuration. Upon further increasing the reverse DC bias, the domain state evolves toward a 180°-domain-dominated configuration, suppressing the shear-mediated contributions and causing d'_{31} to decrease and change sign. At sufficiently large negative bias, the system therefore re-enters an auxetic piezoelectric regime.

The vector PFM measurements used above as experimental constraints also provide direct real-space evidence for this field-driven domain evolution. As shown in Fig. 5(b) and Fig. S17 of the SM, the crystal evolves from a nearly single-domain state to a multi-domain configuration at intermediate bias and finally toward a reversed nearly single-domain state at large negative bias.

To understand the thermodynamic origin of the field-driven domain evolution, we employed Landau phenomenological theory [31−33]. With a DC bias along $[\bar{1}\bar{1}\bar{1}]_{pc}$ applied to the crystal, the free energy of polarizations along $[11\bar{1}]_{pc}$, $[\bar{1}\bar{1}1]_{pc}$, and $[\bar{1}\bar{1}\bar{1}]_{pc}$ all become lower than that of the pristine $[111]_{pc}$ state (see Fig. S18 of the SM). Hessian analysis further confirms that multiple polarization states remain locally stable over an intermediate electric-field range, while their comparable free energies indicate strong thermodynamic competition and establish a thermodynamic basis for multi-variant coexistence [Fig. 5(c) and Fig. S19 of the SM]. We note here that domain-wall energy [15], elastic compatibility [15, 34], defects [35], and kinetic effects [36], which are not explicitly included in the homogeneous Landau model, may further influence how these competing states are spatially accommodated and dynamically realized in the actual crystal. This thermodynamic competition is consistent with the bias-dependent domain evolution observed by vector PFM.

Together, these results establish that the electric-field-driven switching between auxetic and conventional piezoelectric responses in $(111)_{pc}$-oriented PMN-30PT originates from a bias-controlled redistribution of rhombohedral domain variants, and is amplified by the intrinsically large shear coefficient d_{15}. In addition to the domain-variant redistribution captured by the present model, domain-wall motion and domain-size evolution may also contribute to the apparent piezoelectric response during bias-driven domain evolution, as widely reported in ferroelectrics [34, 37−42].

Conclusion

In conclusion, we have demonstrated intrinsic and electrically switchable auxetic piezoelectricity in rhombohedral relaxor ferroelectric PMN-PT using a $(111)_{pc}$-oriented single crystal as a model system. Benefiting from facile electric-field-driven domain reconfiguration, the crystal undergoes a reversible transition between auxetic and conventional piezoelectric states, accompanied by a continuous evolution of the electromechanical ratio v_{13}. The ability to continuously tune v_{13} from negative to zero and positive values provides a practical framework for designing tunable and reconfigurable piezoelectric functionalities. These findings establish domain reconfiguration as an effective strategy for programming unconventional electromechanical responses in relaxor ferroelectrics, opening a pathway toward next-generation reconfigurable piezoelectric devices for tunable transduction, sensing, and energy-harvesting applications.

Author Contributions

M.-M.Y. conceived the idea and supervised the project. H.-M.S., H.-B.Z., and M.-M.Y. designed the experiments. H.-M.S. performed the piezoelectric measurements and structural characterizations, and developed the multi domain model. Z.-T. carried out the first-principles calculations. H.-B.Z. performed the thermodynamic calculations. H.-M.S. and M.-M.Y. wrote the manuscript with contributions from all authors. All authors discussed the experimental results and models, commented on the manuscript, and approved the final version.

Conflict of Interest Statement

None declared.

Acknowledgements

We acknowledge the technical support from Anhui Epitaxy Technology Co., Ltd. This work was partially carried out at the Center for Micro and Nanoscale Research and Fabrication at the University of Science and Technology of China (USTC). This work was supported by the National Key Research and Development Program of China (Grant No. 2025YFE0201100), the Natural Science Foundation of Anhui Province (Grant No. 2508085ZD015), and the National Natural Science Foundation of China (Grant No. 12404110).

References

[1] Li F, Wang B, Gao X, Damjanovic D, Chen L Q, and Zhang S 2025 *Science* **389** eadn4926
[2] Sun E and Cao W 2014 *Prog. Mater. Sci.* **65** 124
[3] Mahapatra S D, Mohapatra P C, Aria A I, Christie G, Mishra Y K, Hofmann S, and Thakur V K 2021 *Adv. Sci.* **8** e2100864
[4] Tang M, Liu X, Bian J, Hu L, Wang Y, Ren X, Wang Y, Zhao H, Priya S, Xu Z, Geng L D, and Yan Y 2025 *Acta Mater.* **296** 121265
[5] Liu J, Liu S, Yang J Y, and Liu L 2020 *Phys. Rev. Lett.* **125** 197601
[6] Peng Y, Deng Z, Song S, Tang G, and Hong J 2025 *Phys. Chem. Chem. Phys.* **27** 10652
[7] Talley K R, Perkins C L, Diercks D R, Brennecka G L, and Zakutayev A 2021 *Science* **374** 1488
[8] Yang M M, Zhu T Y, Renz A B, Sun H M, Liu S, Gammon P M, and Alexe M 2024 *Nat. Mater.* **23** 95
[9] Eliseev E A and Morozovska A N 2024 *Nat. Mater.* **23** 37
[10] Tan Z, Sun H M, Shi W, Guan S, Zhang H, Jiang L, Chen Q, Xing J, Zhu J, and Yang M M. 2026 *Natl. Sci. Rev.* **13** nwag295
[11] Mahmoud A, Erba A, El-Kelany K E, Rérat M, and Orlando R 2014 *Phys. Rev. B* **89** 045103
[12] Zhang S, Li F, Jiang X, Kim J, Luo J, and Geng X 2015 *Prog. Mater. Sci.* **68** 1
[13] Qiu C, Wang B, Zhang N, Zhang S, Liu J, Walker D, Wang Y, Tian H, Shrout T R, Xu Z, Chen L Q, and Li F 2020 *Nature* **577** 350
[14] Fu H and Cohen R E 2000 *Nature* **403** 281
[15] Jin Y M, Wang Y U, Khachaturyan A G, Li J F, and Viehland D 2003 *Phys. Rev. Lett.* **91** 197601
[16] Gonze X and Lee C 1997 *Phys. Rev. B* **55** 10355
[17] Baroni S, de Gironcoli S, Dal Corso A, and Giannozzi P 2001 *Rev. Mod. Phys.* **73** 515
[18] Wu X, Vanderbilt D, and Hamann D R 2005 *Phys. Rev. B* **72** 035105
[19] Sághi-Szabó G, Cohen R E, and Krakauer H 1998 *Phys. Rev. Lett.* **80** 4321
[20] Bernardini F, Fiorentini V, and Vanderbilt D 1997 *Phys. Rev. B* **56** R10024
[21] Mathis M A and Marianetti C A 2024 *Phys. Rev. B* **110** L140101
[22] Rojac T 2023 *Commun. Mater.* **4** 12
[23] Li F, Zhang S, Xu Z, and Chen L Q 2017 *Adv. Funct. Mater.* **27** 1700310
[24] Manley M E, Abernathy D L, Sahul R, Parshall D E, Lynn J W, Christianson A D, Stonaha P J, Specht E D, and Budai J D 2016 *Sci. Adv.* **2** e1501814
[25] Aleshin V I and Raevski I P 2012 *J. Appl. Phys.* **112** 114101
[26] Lim T C 2023 *Int. J. Solids Struct.* **284** 112510
[27] Khan K A and Khan M A 2019 *Mater. Res. Bull.* **112** 194
[28] Yang L, Zhao Y, Zhang S, Li P, Gao Y, Yang Y, Huang H, Miao P, Liu Y, Chen A, Nan C W, and Gao C 2014 *Sci. Rep.* **4** 4591
[29] Zhang R, Jiang B, and Cao W 2003 *Appl. Phys. Lett.* **82** 787
[30] Zhang R, Jiang B, and Cao W 2003 *Appl. Phys. Lett.* **82** 3737
[31] Lu X, Zhang H, Zheng L, and Cao W 2017 *J. Appl. Phys.* **122** 054102
[32] Zhang H, Lu X, Wang R, Wang C, Zheng L, Liu Z, Yang C, Zhang R, Yang B, and Cao W 2017 *Phys. Rev. B* **96** 054109
[33] Zhang H, Lu X, Wang C, Zheng L, Yang B, and Cao W 2018 *Phys. Rev. B* **97** 054114
[34] Catalan G, Seidel J, Ramesh R, and Scott J F 2012 *Rev. Mod. Phys.* **84** 119
[35] Ren X 2004 *Nat. Mater.* **3** 91
[36] Tybell T, Paruch P, Giamarchi T, and Triscone J M 2002 *Phys. Rev. Lett.* **89** 097601
[37] Xu R, Karthik J, Damodaran A R, and Martin L W 2014 *Nat. Commun.* **5** 3120
[38] Liu L, Rojac T, Damjanovic D, Di Michiel M, and Daniels J 2018 *Nat. Commun.* **9** 4928
[39] Kim S, Miyauchi R, Sato Y, Nam H, Fujii I, Ueno S, Kuroiwa Y, and Wada S 2023 *Adv. Mater.* **35** e2208717
[40] Ghosh D, Sakata A, Carter J, Thomas P A, Han H, Nino J C, and Jones J L 2013 *Adv. Funct. Mater.* **24** 885
[41] Wang B, Li F, and Chen L Q 2021 *Adv. Mater.* **33** 2105071
[42] Bell A J, Shepley P M, and Li Y 2020 *Acta Mater.* **195** 292